J. Fluid Mech. (2010), *vol.* 642, *pp.* 395–420.
doi:10.1017/S0022112009991820

Statistics of surface gravity wave turbulence in the space and time domains

SERGEY NAZARENKO[1], SERGEI LUKASCHUK[2]†, STUART McLELLAND[3] AND PETR DENISSENKO[4]

[1]Mathematics Institute, Warwick University, Coventry CV4 7AL, UK

[2]Department of Engineering, Hull University, Hull HU6 7RX, UK

[3]Department of Geography, Hull University, Hull HU6 7RX, UK

[4]School of Engineering, Warwick University, Coventry CV4 7AL, UK

(Received 1 April 2009; revised 24 August 2009; accepted 27 August 2009; first published online 9 December 2009)

We present experimental results on simultaneous space–time measurements for the gravity wave turbulence in a large laboratory flume. We compare these results with predictions of the weak turbulence theory (WTT) based on random waves, as well as with predictions based on the coherent singular wave crests. We see that the both wavenumber and frequency spectra are not universal and dependent on the wave strength, with some evidence in favour of the WTT at larger wave intensities when the finite-flume effects are minimal. We present further theoretical analysis of the role of the random and coherent waves in the wave probability density function (p.d.f.) and the structure functions (SFs). Analysing our experimental data we found that the random waves and the coherent structures/breaks coexist: the former show themselves in a quasi-Gaussian p.d.f. core and the low-order SFs and the latter in the p.d.f. tails and the high-order SFs. It appears that the x-space signal is more intermittent than the t-space signal, and the x-space SFs capture more singular coherent structures than the t-space SFs do. We outline an approach treating the interactions of these random and coherent components as a turbulence cycle characterized by the turbulence fluxes in both the wavenumber and the amplitude spaces.

Key words: surface gravity waves, wave breaking, wave–turbulence interactions

1. Introduction

Understanding statistics of random water surface waves and their mutual nonlinear interaction mechanisms is important for wave forecasting and weather and climate modelling (see for example Janssen 2004). Field observations of the sea surface, laboratory experiments in wave flumes and numerical simulations are efficient and complimentary tools for studying such random nonlinear waves and for testing existing theoretical models. The obvious advantage of the field observations is that they deal directly with the system we want to know about, rather than modelling it in a scaled-down laboratory experiment or in numerical simulation. In comparison with field measurements, laboratory experiments and numerical simulations allow more control over the physical conditions and over the quantities we measure, especially in the numerical simulations, which allows us to access a much broader range of diagnostics than that in experiments.

† Email address for correspondence: S.Lukaschuk@hull.ac.uk

On the other hand, the laboratory experiments enable observations of much larger range of wave scales than is possible in numerical simulations under the current level of resolution, and therefore, they allow one to obtain cleaner power-law spectra and other scalings. Furthermore, laboratory experiments are much more realistic than numerics in reproducing the strongly nonlinear events because most numerical methods are based on weakly nonlinear truncations of the original fluid equations. Finally, they also have a natural dissipation mechanism as in open seas, namely wave breaking, in contrast with an artificial hyper-viscous dissipation which is usually used in numerics.

In the present paper, we report on new experimental results in a laboratory flume of dimensions $12 \times 6 \times 1.5\,\mathrm{m}$. In our previous experiments at the same facility (Denissenko, Lukaschuk & Nazarenko 2007) we measured the time series of the surface elevation at several fixed locations on the two-dimensional plane, using point-like wire capacitance probes. This is a standard technique which was also used in the smaller experiments of Falcon, Laroche & Fauve (2007) and which allows one to obtain the wave spectra in the frequency domain, as well as higher-order statistics of the surface heights from the time series acquired at fixed spatial locations. For weakly nonlinear waves, such measurements seem to be sufficient for obtaining information about the space distributions of the waves (e.g. the wavenumber spectra) via the linear wave dispersion relation $\omega = \sqrt{gk}$. On the other hand, our previous experimental results (Denissenko *et al.* 2007) indicated that in the laboratory flumes there are significant finite-size effects which can be overcome only at rather high levels of nonlinearity of the wave field. In particular, at high averaged wave field intensities we observed a better agreement with the ω^{-4} prediction of the Zakharov–Filonenko (ZF) wave turbulence theory (Zakharov & Filonenko 1967; Zakharov, Lvov & Falkovich 1992) developed for weakly nonlinear waves with almost random phases. On the other hand, the same ω^{-4} spectrum was predicted by the theory of Kuznetsov (2004) based on the assumption that the dominant contribution to the power-law scaling comes from sharp wave crests with one-dimensional ridges whose velocity remains nearly constant while crossing the wire probe (we denote these results as the Kuznetsov theory or Kuznetsov spectrum). Obviously, the nonlinearity of such wave crests is high, and one cannot use the linear dispersion relation for obtaining the space statistics out of the time statistics. It is worth mentioning that the ω^{-4} spectrum was first put forward based on a simple dimensional argument and experimental data by Kitaigorodskii (1962) and was later obtained in a similar way by Toba (1973). In the water wave literature it is often called the Toba spectrum, and its interpretations frequently differ from the ZF or Kuznetsov mechanisms described above. This situation demonstrates that the frequency spectrum alone does not allow us to distinguish between such drastically different types of waves, i.e. random-phased modes and sharp-crested structures. On the other hand, the ZF and Kuznetsov theories predict very different shape of the k-spectra, namely $k^{-2.5}$ (for one-dimensional spectral density) versus k^{-4} respectively. Thus, a direct method of measuring the k-spectra could allow one to differentiate between the ZF and Kuznetsov states.

A fractal distribution of coherent wave-breaking events, which is even more complicated and leads to the same ω-spectrum and k-spectrum as in the Kuznetsov theory, was put forward by Belcher & Vassilicos (1997). Thus, measuring the k-spectrum along with the ω-spectrum answers many but not all of the questions about the structure of the wave field. However, random waves and coherent structures/breaks of different kinds have different signatures in the high-order statistics of the wave elevations. It is well known, for example, that wave breaking

may be of different kinds, ranging from the progressive-wave breaks with a limiting angle of 120° typical for the open seas to vertical-jet ejections typical of the breaking of standing waves or waves reflected from walls (Cooker & Peregrine 1991; Longuet-Higgins 1993). In laboratory flumes, it is not *a priori* clear which kind will dominate because the sufficiently large nonlinearity leading to breaking at the same time leads to wave decorrelations and the respective departure from the standing-wave structure of the linear eigenmodes. To find which breaking type dominates, one can look for its signature in the high-order statistics.

We would like to emphasize that even for wave fields which are weakly nonlinear on average, occasional strongly nonlinear wave crests and wave breaks are known to occur. In spite of being seldom, these structures are crucial because they provide the main mechanism for dissipation of the wave energy, and they are related to the phenomenon of intermittency in wave turbulence. After wave breaking, such structures loose their ability to maintain coherence, and part of their energy returns to the random wave component. Thus, a realistic description of the wave turbulence should include two equally important components, the random waves and the coherent structures, which interact and get transformed into one another during different parts of the wave turbulence life cycle. Again, since the seldom breaking events are strongly nonlinear, one cannot use the linear dispersion relation for understanding their statistics, and a direct x-space measurement is desirable.

With these motivations in mind, in the present work we have implemented a new technique for direct one-dimensional measuring of instantaneous surface profiles (see the details below). Thus, we are able to measure the k-spectra directly, as well as the higher-order x-space statistics averaged over a discrete set of instants of time, particularly the probability density functions (p.d.f.s) and structure functions (SFs) of the height increments in space. This can be done at different levels of wave forcing, but we have excluded the range of very weak forcing for which the finite-flume-size effects were shown to be significant. This was primarily to achieve better scaling regimes, since at low intensities the spectra are very steep and span over smaller ranges of scales with some peaks often obscuring the power-law fits (Denissenko *et al.* 2007). The x-space measurements are accompanied by the capacitance fixed-point measurements of the t-series for the same experimental runs, which gives us simultaneous information about the space- and time-domain statistics of the water surface elevation.

The main message of the present paper is that the wave turbulence behaviour is typically non-universal and reflects the presence of two coexisting species, namely weak incoherent waves and sparse but strong sharp wave-crest structures. The incoherent waves dominate in the spectra and the scalings of the low-order SFs. These scaling agree with ZF weak turbulence predictions for the spectra at higher amplitudes. Moreover, we see consistency with ZF scalings for the low-order SFs at relatively high amplitudes (when the finite-size effects are minimal). Further, the ZF theory appears to agree better with the t-domain than ω-domain statistics, which is clearly the finite-inertial-range effect (because the t- and the ω-objects are related via the Fourier transform). For the higher-order SFs, we see behaviour characteristic of intermittency and presence of singular coherent structures. Interestingly, propagating Kuznetsov-type one-dimensional wave crests are better detected by the t-space SFs, and the x-space SFs capture more singular, almost non-propagating wave crests schematically shown in figure 1.

Our paper is organized as follows. In § 2 we describe the relevant theories and predictions for the surface-wave turbulence. In § 3 we describe the experimental

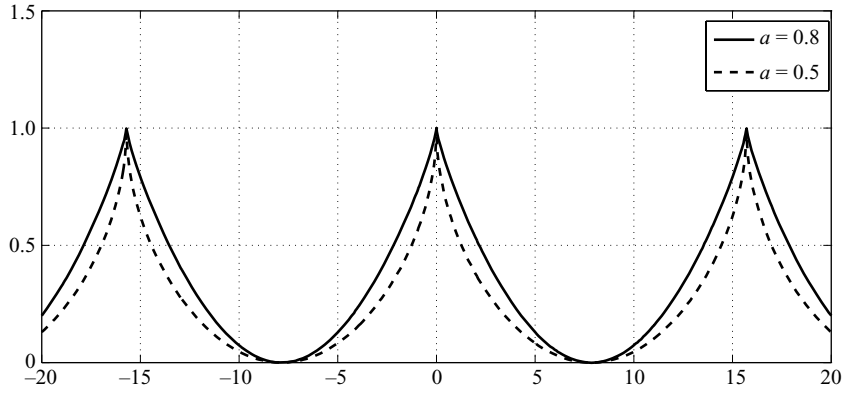

FIGURE 1. A wave profile with singular structures of the type $\eta(x) = \eta_0 - C_a\,|x|^a$ with $0 < a < 1$. (The plot shows $y = 1 - |\sin(0.2x)|^a$.)

facility and the measurement techniques. In § 4 we present the experimental results along with their discussion in the context of the theoretical predictions and possible interpretations. In § 5 we present a summary of our findings and an outlook for future work.

2. Theoretical background

Let us start with a theoretical background including an overview of the existing theoretical predictions as well as a further analysis of the statistical objects relevant to our experiments.

2.1. *Spectra*

First, let us define the wave energy spectrum in the frequency domain as

$$E_\omega = \int \mathrm{e}^{\mathrm{i}\omega t'} \langle \eta(\boldsymbol{x}, t)\eta(\boldsymbol{x}, t + t')\rangle \,\mathrm{d}t' \tag{2.1}$$

and the one-dimensional energy spectrum in the wavenumber domain as

$$E_k = \int \mathrm{e}^{\mathrm{i}kz} \langle \eta(\boldsymbol{x}, t)\eta(\boldsymbol{x} + \boldsymbol{w}z, t)\rangle \,\mathrm{d}z, \tag{2.2}$$

where $\eta(\boldsymbol{x}, t)$ is the surface elevation at time t and the location in the horizontal plane $\boldsymbol{x} = (x, y)$. The integration in (2.1) is taken over a time window, and that in (2.2) is taken over an interval of a straight line in the two-dimensional plane illuminated by the laser sheet (with $\boldsymbol{w}$ being a unit vector along this line). The angle brackets mean ensemble averaging over realizations (equivalent to the time averaging in presence of ergodicity). For a statistically steady and homogeneous state, E_ω and E_k are independent of t and $\boldsymbol{x}$. Most of the theories predict power-law scalings,

$$E_\omega \propto \omega^{-\nu} \tag{2.3}$$

and

$$E_k \propto k^{-\mu}, \tag{2.4}$$

where the indices ν and μ depend on a particular theory.

2.2. *Statistics of the field increments*

The spectra considered in the previous section correspond to the second-order correlators. Different types of coherent and incoherent structures may lead to the same spectra. One, therefore, must consider higher-order correlators to see an unequivocal signature of a particular kind of coherent structures or incoherent random-phased field.

To study the higher-order statistics in our previous paper (Denissenko *et al.* 2007) we considered the p.d.f.s of the wave-crest heights, as well as the p.d.f.s of a band-pass-filtered field (the theory for the latter was developed in Choi *et al.* 2005). Here, we will also consider other objects (which are very popular in turbulence theory): space and time elevation field increments of different orders, which are defined as

$$\delta_l^{(1)} = \eta(\boldsymbol{x} + \mathbf{l}) - \eta(\boldsymbol{x}), \tag{2.5}$$

$$\delta_l^{(2)} = \eta(\boldsymbol{x} + \mathbf{l}) - 2\eta(\boldsymbol{x}) + \eta(\boldsymbol{x} - \mathbf{l}) \tag{2.6}$$

and so on (here all values of η are taken at the same t), and

$$\delta_\tau^{(1)} = \eta(t + \tau) - \eta(t), \tag{2.7}$$

$$\delta_\tau^{(2)} = \eta(t + \tau) - 2\eta(t) + \eta(t - \tau) \tag{2.8}$$

and so on (here all values of η are taken at the same $\boldsymbol{x}$).

2.2.1. *Probability density functions*

The p.d.f.s of the above increments, $P_x(\sigma)$ and $P_t(\sigma)$, are defined in the usual way as a probability of a particular increment in the range from σ to $\sigma + d\sigma$ divided by $d\sigma$, or in the symbolic form as

$$P_x^{(j)}(\sigma) = \left\langle \delta\left(\sigma - \delta_l^{(j)}\right)\right\rangle \tag{2.9}$$

and

$$P_t^{(j)}(\sigma) = \left\langle \delta\left(\sigma - \delta_\tau^{(j)}\right)\right\rangle \tag{2.10}$$

respectively, where $j = 1, 2, \ldots$ and $\delta(x)$ is Dirac's delta-function ((2.9) and (2.10) are related to the obvious identity $\langle f(\sigma)\rangle \equiv \int f(\sigma')P(\sigma')\,\mathrm{d}\sigma' = \int f(\sigma')\langle\delta(\sigma - \sigma')\rangle\,\mathrm{d}\sigma' = \langle f(\sigma)\rangle$). For random-phased fields, these p.d.f.s are Gaussian, and presence of sparse coherent structures can be detected by the deviations from Gaussianity at the p.d.f. tails. In particular, fatter-than-Gaussian tails indicate an enhanced probability of strong bursts in the signal, which is called intermittency.

2.2.2. *Structure functions*

Let us now introduce the moments of the height increments, which are called the 'structure functions',

$$S_l^{(j)}(p) = \left\langle \left(\delta_l^{(j)}\right)^p \right\rangle = \int \sigma^p P_x^{(j)}(\sigma)\,\mathrm{d}\sigma \tag{2.11}$$

and

$$S_\tau^{(j)}(p) = \left\langle \left(\delta_\tau^{(j)}\right)^p \right\rangle = \int \sigma^p P_t^{(j)}(\sigma)\,\mathrm{d}\sigma. \tag{2.12}$$

Often in turbulence, the SFs asymptotically tend to scaling laws,

$$S_l^{(j)}(p) \sim l^{\xi(p)} \tag{2.13}$$

in the limit $l \to 0$ and

$$S_\tau^{(j)}(p) \sim \tau^{\zeta(p)} \tag{2.14}$$

in the limit $\tau \to 0$. Functions $\xi(p)$ and $\zeta(p)$ are called the SF scaling exponents, and they contain the most important information about the coherent and incoherent components of the turbulent field and, correspondingly, about the turbulence intermittency.

2.3. *Scalings generated by random-phased waves*

2.3.1. *Spectra*

The weak turbulence theory (WTT) considers weakly nonlinear random-phased waves in an infinite-box limit. For the wave spectrum, these assumptions lead to the so-called Hasselmann equation (Hasselman 1962),

$$\dot{n}_k = 4\pi \int |W(\boldsymbol{k}, \boldsymbol{k}_1, \boldsymbol{k}_2, \boldsymbol{k}_3)|^2 \delta(\boldsymbol{k} + \boldsymbol{k}_1 - \boldsymbol{k}_2 - \boldsymbol{k}_3)\delta(\omega_k + \omega_{k_1} - \omega_{k_2} - \omega_{k_2}) \times n_k n_{k_1} n_{k_2} n_{k_3} \left(\frac{1}{n_k} + \frac{1}{n_{k_1}} - \frac{1}{n_{k_2}} - \frac{1}{n_{k_3}} \right) \mathrm{d}\boldsymbol{k}_1 \, \mathrm{d}\boldsymbol{k}_2 \, \mathrm{d}\boldsymbol{k}_3, \quad (2.15)$$

where $n_k = E_k/(2\pi k \omega_k)$ is the wave-action spectrum and $W(\boldsymbol{k}, \boldsymbol{k}_1, \boldsymbol{k}_2, \boldsymbol{k}_3)$ is the interaction coefficient given by a rather lengthy expression which can be found in Krasitskii (1994).

The Hasselmann equation has an exact power-law solution,

$$E_k \propto k^{-5/2} \quad (2.16)$$

or

$$E_\omega \propto \omega^{-4} \quad (2.17)$$

in the ω-domain. This solution is called the ZF energy spectrum, and it describes a steady state with energy cascading through an inertial range of scales from large scales, where it is produced, to the small scales, where it is dissipated by wave breaking.

It is important that in deriving the WTT, the limit of an infinite box is taken before the limit of small nonlinearity. This means that in a however-large but finite box, the wave intensity should be strong enough for the nonlinear resonance broadening to be much greater than the spacing of the k-grid (corresponding to Fourier modes in a finite rectangular box). As estimated by Nazarenko (2006), this implies a condition on the minimal angle of the surface elevation $\gamma > 1/(kL)^{1/4}$, where L is the size of the basin, which is quite a severe restriction. If this condition is not satisfied the number of exact and quasi-four-wave resonances will be drastically depleted (Kartashova 1991, 1998; Nazarenko 2006). This can lead to a significant slowdown of the energy cascade from long to short waves and, therefore, a steeper energy spectrum. A theory of discrete wave turbulence developed by Nazarenko (2006) for very low levels of forcing predicts $E_\omega \propto \omega^{-6}$, which is confirmed in experiments with very weak forcing (Denissenko *et al.* 2007). On the other hand, for such weak forcing the scaling interval is rather short and not very well formed (it contains some peaks). Thus, in the present paper we will deal with stronger wave fields for which the spectra are shallower ($\nu \lesssim 5.5$), even though they are still steeper than the ZF ones owing to the finite-size effects.

2.3.2. *The probability density functions and the structure functions*

Now let us consider a wave field made out of modes with random phases and the energy spectrum $E_k \sim k^{-\mu}$. As we mentioned, for random-phased fields, the p.d.f.s of the height increments are Gaussian. For Gaussian statistics we immediately have

$$S_l^{(j)}(p) \sim l^{p(\mu-1)/2} \quad (2.18)$$

if $\mu < 2j+1$; otherwise $S_l^{(j)}(p) \sim l^{pj}$ because the field is j times differentiable.

Similarly, in the time domain for the random-phased field with the energy spectrum $E_\omega \sim \omega^{-\nu}$ we have

$$S_\tau^{(j)}(p) \sim \tau^{p(\nu-1)/2} \tag{2.19}$$

if $\nu < 2j+1$; otherwise $S_\tau^{(j)}(p) \sim \tau^{pj}$.

2.4. *Scalings generated by singular coherent structures*

2.4.1. *Spectra*

Sharp wave crests are quite common for gravity waves of sufficiently large amplitudes. The most common type of crests discussed in the literature look like a break in the surface slope. A prototype for such structures is a sharp-crested stationary Stokes wave solution with the crest angle of 120°. Following Kadomtsev (1965), such sharp-crested waves are usually associated with the Phillips spectrum. Indeed, let us assume that there are discontinuities occurring at isolated points. This leads to the following one-dimensional energy spectrum in wavenumber space:

$$E_k \propto k^{-3}. \tag{2.20}$$

Second, assuming that transition from the k-space to the ω-space should be done according to the linear wave relation $\omega = \sqrt{gk}$, we arrive at the Phillips spectrum (Phillips 1958),

$$E_\omega \sim g^2 \omega^{-5}. \tag{2.21}$$

An alternative way to derive the Phillips spectrum, the way it was originally done by Phillips, is to assume that the gravity constant g is the only relevant dimensional physical quantity. This argument is equivalent to saying that the linear term is of the same order as the nonlinear one in the water surface equations in the Fourier space.

Kuznetsov (2004) questioned this picture and argued (i) that slope breaks occur on one-dimensional lines/ridges rather than on zero-dimensional point/peaks and (ii) that the wave crest is propagating with preserved shape, or in other words $\omega \propto k$ should be used instead of the linear wave relation $\omega = \sqrt{gk}$. These assumptions give $E_\omega \propto \omega^{-4}$, i.e. formally the same scaling as ZF, even though the physics behind it is completely different. Finally, it was proposed by Connaughton, Nazarenko & Newell (2003) that wave-crest ridges may have non-integer fractal dimension D somewhere in the range $0 < D < 2$. This leads to the following one-dimensional energy spectrum in the k-space:

$$E_k \propto k^{-3-D}. \tag{2.22}$$

If we assume, following Kuznetsov, that $\omega \propto k$, we have

$$E_\omega \propto \omega^{D-6}. \tag{2.23}$$

2.4.2. *The structure functions and the probability density functions*

Let us now consider a somewhat more general class of singular coherent structures whose cross-section near the singularity is given by

$$\eta(x) = \eta_0 - C_a |x|^a, \tag{2.24}$$

with a singularity degree constant a such that $0 < a \leqslant 1$ and with constants η_0 and C_a describing a reference surface elevation and the coherent structure amplitude respectively (see figure 1). For the special case of the Phillips and Kuznetsov structures we have $a = 1$. We will see below that structures with the additional parameter $a < 1$

also seem to be relevant to the wave turbulence in our experiments. Further, for the singularity dimension we have $D=0$ for the Phillips structures and $D=1$ for the Kuznetsov structures. In general we will assume that the ridges of such crests may have a fractal dimension $0 \leqslant D < 2$.

In the Appendix we show that the singular structures of type (2.24) give the following contributions to the SFs:

$$S_l^{(j)}(p) \sim l^{pj} + Nl^{2-D+ap}. \tag{2.25}$$

Note that in the limit $l \to 0$ out of the two terms on the right-hand side the one with the smallest power will be dominant, and only in this limit the direct sum in (A 5) is valid (as we explain in the Appendix). Thus, the structures of the Phillips or Kuznetsov type, i.e. with $a=1$, will not bee seen in the SFs for the first-order increments, and we would have to consider $j \geqslant 2$. However, one should keep in mind that the finite range of excited scales makes determination of the scalings less precise for j at higher orders because of the higher number of SF points to be placed in this finite range. Therefore, it is better to consider the lowest j that would allow the extraction of the scalings induced by the coherent structures ($j=2$ in case of Phillips and Kuznetsov).

In the Appendix we also show that the singular structures of type (2.24) with $a=1$ give rise to the following asymptotic behaviour for the p.d.f. tails, $|\sigma| \ll 2l$:

$$P_x^{(2)}(\sigma) \sim \frac{A}{l}\left[\ln\left(\frac{l}{|\sigma|}\right) + B\right], \tag{2.26}$$

where A and B are dimensionless constants which depend on the strength distribution of the singular ridges and their spatial density.

For $a<1$, the singular structures contribute to the p.d.f. tails locally, i.e. forming a non-universal bump on the tail near $\sigma = C_a l^a$.

Now suppose that the wave field is bi-fractal and consists of two components, namely random-phased modes and singular coherent structures. Avoiding the choices of j for which the field is j times differentiable, we have in this case

$$S_l^{(j)}(p) \sim l^{p(\mu-1)/2} + l^{2-D+ap}. \tag{2.27}$$

If $a<(\mu-1)/2$ we expect to see the scaling associated with the incoherent random-phased component at low values of p (first term on the right-hand side) and the singular coherent structure scaling at high values of p (second term on the right-hand side).

Similarly, one can consider the SFs of the time increments. If we assume following Kuznetsov that the coherent structures could be thought as passing the wire probes with constant velocity (owing to shortness of the time needed for the singular ridge to pass the probe), we would obtain the time-domain scalings that are identical to the space-domain scalings obtained above, i.e. $S_\tau^{(j)}(p) \sim \tau^{2-D+ap}$.

In the case in which incoherent waves and singular coherent structures are present simultaneously, we have

$$S_\tau^{(j)}(p) \sim \tau^{p(\nu-1)/2} + \tau^{2-D+ap}. \tag{2.28}$$

As before, it is understood here that the order j is chosen in such a way that the field associated with the incoherent wave component is not j times differentiable in time. For example, for spectra with $3<\nu<5$ (such as for the ZF spectrum) one should use $j \geqslant 2$; for $5<\nu<7$ one should use $j \geqslant 3$; and so on.

2.5. *Bound modes and statistics of the height elevations*

Often in the literature, deviations of the wave fields from the Gaussian statistics are discussed in terms of the 'bound modes'. The concept of the bound modes is the most clear in the weakly nonlinear case, i.e. when the WTT is applicable. Recall that the WTT deals with random-phased waves. However, the normal variables describing the wave amplitudes (the wave-action variables) are related to the physical variables (i.e. the surface elevation and the surface velocity) via a weakly nonlinear canonical transformation. Because of the nonlinearity of this transformation, at a fixed wavenumber $\boldsymbol{k}$ in addition to the main mode frequency $\omega = \omega_k$ there will be secondary frequency components, which are referred to as the bound modes. On the other hand, the nonlinearity of the transformation results in non-Gaussianity of the physical variables. Tayfun distribution is a p.d.f. for the surface elevations, which takes into account such non-Gaussianity and which was derived for weakly nonlinear narrowband spectra (Tayfun 1980; Socquet-Juglard *et al.* 2005; Onorato *et al.* 2009),

$$P_{Tayfun}(\eta) = \frac{1 - 7\sigma^2 k_*^2/8}{\sqrt{2\pi(1 + 3G + 2G^2)}} \exp\left(-\frac{G^2}{2\sigma^2 k_*^2}\right), \tag{2.29}$$

where

$$G = \sqrt{1 + 2\sigma k_*^2 \eta} - 1; \tag{2.30}$$

σ is the standard deviation of η; and k_* is a characteristic wavenumber.

Tayfun distribution appears to be a reasonable qualitative model for broadband spectra too (Onorato *et al.* 2006*b*, 2009; Denissenko *et al.* 2007; Tayfun & Fedele 2007) (in which case wavenumber k_* is a fitting parameter), and it is often used to quantify the appearance of 'freak' waves whose height is significantly greater than the average wave elevation (Janssen 2004; Onorato *et al.* 2006*b*, 2009; Tayfun & Fedele 2007).

Two global parameters which could be obtained from the elevation p.d.f. and which are often used as indicators of deviation from Gaussianity are the skewness $C_3 = \langle \eta^3 \rangle / \langle \eta^2 \rangle^{3/2}$ and the kurtosis $C_4 = \langle \eta^4 \rangle / 3\langle \eta^2 \rangle^2 - 1$.

It should be clear that the bound modes and the singular coherent structures are not totaly different objects, and on the contrary, they are closely related. One can qualitatively think of the same type of nonlinear Stokes waves, for which the bound modes provide an effective description for weaker nonlinearities, and the singular profiles appear for the strongest possible nonlinearity corresponding to 120° crests. In fact, the strongly nonlinear coherent waves, including those with profiles close to the singular, are often also referred to as the 'bound' waves to distinguish them from the 'free' waves whose phases are uncorrelated.

Let us discuss the relation between the statistics of the surface elevations measured at a single point (to which the Tayfun distribution is intended) and the statistics of the multi-point increments introduced in the previous section. Obviously, when the separation of the points in the increment is greater than the wave correlation length, then the multi-point p.d.f. factorizes in terms of the one-point p.d.f.s. Thus, in the large-l limit the multi-point and one-point p.d.f.s contain the same information. On the other hand, for small l the elevation increments are related to the derivatives of the height elevation; e.g. $\delta_l^{(1)}$ measure the slope and $\delta_l^{(2)}$ measure the curvature. Thus, using $\delta_l^{(2)}$ allows one to pick out singular points with high curvature and magnify their effect by choosing high-order p of the SFs. On the other hand, the effect of the weakly nonlinear bound modes on the statistics of such increments is expected

to remain sub-dominant because they do not lead to the high-curvature points. Indeed, provided the nonlinearity remains weak in the scales which give dominant contribution to curvature, the bound modes will remain a perturbation at these scales; i.e. the curvature distribution will be close to the one of a Gaussian field. If, on the other hand, the curvature-dominated scales are strongly nonlinear, then the perturbative bound mode approach is invalid, and we are again in the situation in which the singular coherent structures are more relevant.

We can summarize that the single-point elevation p.d.f.s are directly relevant to the rogue-wave phenomenon for which the bound modes are essential, whereas the multi-point p.d.f.s of the elevation increments are more suited for detecting singularities associated with wave breaking.

2.6. *Turbulence cycle and fluxes in the wavenumber–amplitude space*

In the previous sections we used the Fourier space for the spectra, whereas the higher-order statistics was described in terms of the x- and t-domain increments. In this subsection, we will outline how one can put turbulence containing incoherent waves and coherent structures on to the same 'map'. Namely, we will be interested in a turbulence cycle in which the structures arise from the turbulent cascade of incoherent waves and, in turn, incoherent waves arise during breaking of the structures. The key element of this picture is combining fluxes over wavenumbers (associated with the Kolmogorov–Zakharov cascade states) and over the wave amplitudes (considered by Choi *et al.* 2005 and linked to intermittency).

Let us summarize the findings of Choi *et al.* (2005), where the WTT formalism was extended to the p.d.f. of Fourier intensities $J_k = |a_k|^2$, which is defined as

$$\mathscr{P}_k(J) = \langle \delta(J - |a_k|^2) \rangle. \tag{2.31}$$

Under the usual WTT assumptions (weak nonlinearity, random phases and amplitudes of the Fourier modes), the following equation for such a p.d.f. was derived:

$$\dot{\mathscr{P}} + \partial_J F = 0, \tag{2.32}$$

where

$$F = -J(\beta \mathscr{P} + \alpha \partial_J \mathscr{P}) \tag{2.33}$$

is a probability flux in the J-space and

$$\alpha_k = 4\pi \int |W(\boldsymbol{k}, \boldsymbol{k}_1, \boldsymbol{k}_2, \boldsymbol{k}_3)|^2 \delta(\boldsymbol{k} + \boldsymbol{k}_1 - \boldsymbol{k}_2 - \boldsymbol{k}_3) \delta(\omega_k + \omega_{k_1} - \omega_{k_2} - \omega_{k_2}) \times n_{k_1} n_{k_2} n_{k_3} \, \mathrm{d}\boldsymbol{k}_1 \, \mathrm{d}\boldsymbol{k}_2 \, \mathrm{d}\boldsymbol{k}_3, \tag{2.34}$$

$$\beta_k = 8\pi \int |W(\boldsymbol{k}, \boldsymbol{k}_1, \boldsymbol{k}_2, \boldsymbol{k}_3)|^2 \delta(\boldsymbol{k} + \boldsymbol{k}_1 - \boldsymbol{k}_2 - \boldsymbol{k}_3) \delta(\omega_k + \omega_{k_1} - \omega_{k_2} - \omega_{k_2}) \times [n_{k_1}(n_{k_2} + n_{k_3}) - n_{k_2} n_{k_3}] \, \mathrm{d}\boldsymbol{k}_1 \, \mathrm{d}\boldsymbol{k}_2 \, \mathrm{d}\boldsymbol{k}_3,$$

with $n_k = \langle J \rangle$ and $W(\boldsymbol{k}, \boldsymbol{k}_1, \boldsymbol{k}_2, \boldsymbol{k}_3)$ the nonlinearity coefficient which for the case of the surface gravity waves can be found in the work of Krasitskii (1994). It was shown that there are solutions for such wave p.d.f.s that have power-law tails and, therefore, correspond to the states with turbulent intermittency. These solutions correspond to a constant J-flux of probability, $F = \text{const}$. At the tail of the p.d.f., $J \gg \langle J \rangle = n_k$, the solution can be represented as series in n_k/J,

$$\mathscr{P}_k(J) = -F/(J\beta) - \alpha F/(\beta J)^2 + \cdots. \tag{2.35}$$

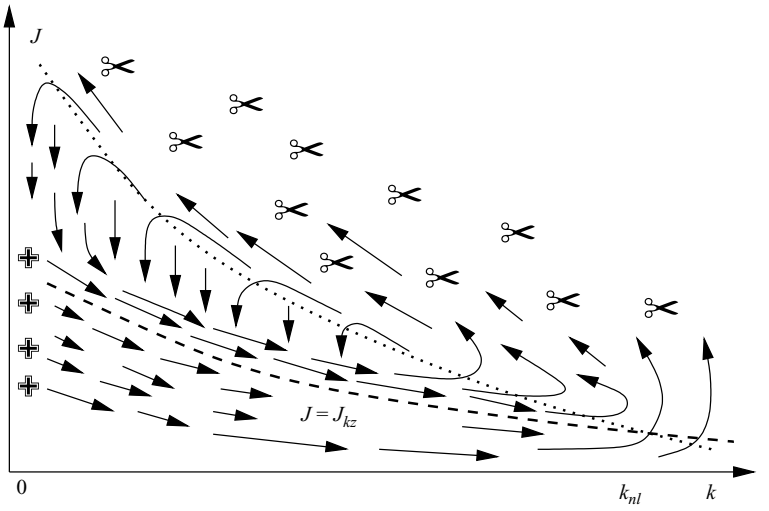

FIGURE 2. Turbulent probability fluxes in the (k, J)-plane. The ZF spectrum, $J(k) = J_{ZF}(k) \sim \epsilon^{1/3}k^{-4}$, and the Phillips spectrum, $J_{Ph} \sim g^{1/2}k^{-9/2}$, are shown by the dashed and the dotted line respectively. The forcing and dissipation regions are marked by the 'plus' and 'scissor' symbols respectively.

It was speculated that such a flux in the amplitude space can be physically generated by the wave-breaking events. On the other hand, we know that the ZF state (and, in general, the Kolmogorov–Zakharov spectrum in other applications) corresponds to the energy flux through wavenumbers k. Below, we will consider a combined flux which has both k and J components and, thereby, clarify the picture of the wave turbulence cycle which involves both random waves and coherent structures that can get transformed into each other.

First note that the situation is quite subtle because the intermittent solution corresponds to the negative J-flux, i.e. from large to small amplitudes, whereas naively one would expect the opposite direction based on the picture that wave breaking occurs and dissipates turbulence when amplitudes become large. To resolve this 'paradox', one should remember that when amplitudes become large the all k-modes become correlated (i.e. we observe occurrence of the coherent structures). Namely, these modes are concentrated at the following lines in the (k, J)-plane:

$$J_{Ph} \sim g^{1/2}k^{-9/2}$$

(see figure 2). Note that the subscript 'Ph' here stands for Phillips to emphasize that it corresponds to the Phillips scaling following from (2.20). Note that in the Phillips spectrum the linear and nonlinear time scales are of the same order, which implies the presence of coherent structures whose Fourier components have correlated phases. Let us consider the fluxes in the (k, J)-plane. Let us force turbulence by generating weak waves at low values of k – the region marked by the 'plus' symbols in figure 2. The energy cascade will proceed from the forcing region to higher k predominantly along the curve $J(k) = \langle J_k \rangle = n_k$. For example, for the ZF state this curve is

$$J(k) = J_{ZF}(k) \sim \epsilon^{1/3}k^{-4},$$

which immediately follows from (2.16).

Around some scale k_{nl}, where the Phillips and ZF curves intersect, the WTT description breaks down because the nonlinear term becomes of the same order as the linear one. At this point, the phases get correlated, which arises in the form of coherent structures in the x-space. Such coherent structures are made of a broad range of Fourier modes which are correlated and each of which has the linear and nonlinear terms in balance. Indeed, if the linear term for some k was greater than the nonlinear term, then this wave would quickly decorrelate from the rest of the modes. If, on the other hand, the nonlinear term were to get larger than the linear one at some k, then the inertial forces on a fluid element would get larger than the gravity force, and this fluid element would separate from the surface and exit the coherent structure. However, such sea spray and foam do form occasionally via wave breaking, which provides the main mechanism of the wave energy dissipation (marked by the 'scissor' symbols in figure 2). Thus, in the (k, J)-plane, the flux turns at k_{nl} and goes back to lower values of k along the Phillips curve, with some energy lost to the regions above the Phillips curve via wave breaking. Occasionally, the coherent structures lose their coherence owing to the energy loss to the sea spray and foam and the corresponding reduction in nonlinearity. Additional mechanisms that can promote decorrelation of coherent structures are due to their mutual interactions and their interactions with the incoherent component. In the (k, J)-plane, this corresponds to turning of the flux down below the Phillips curve and towards the ZF curve. This closes the cycle of the wave turbulence, in which the energy cascade of the random-phased waves leads to creation of coherent structures, which in turn break down with their energy partially dissipated in whitecapping and partially returned into the incoherent random-phased component. The exact partition of the energy dissipated versus the energy returned to the random waves is not known, but it is natural to think that these parts are of the same order of magnitude.

The last part of the wave turbulence cycle is crucial for understanding intermittency. Indeed, this part corresponds to a flux in the opposite J-direction, which, as we mentioned, corresponds to the power-law tails of the p.d.f. of the Fourier modes.

Note that the picture of the wave turbulence cycle similar to the one described above was previously suggested in the work of Dyachenko *et al.* (1992) in the context of the inverse cascade in optical wave turbulence in the nonlinear Schrödinger model with focusing nonlinearity (see also a detailed description in the concluding section of the paper by Newell, Nazarenko & Biven 2001 and in a recent paper by Newell & Zakharov 2008). In this case, the inverse wave-action cascade proceeds within the incoherent weakly nonlinear wave component until it reaches some (low) wavenumbers at which the nonlinearity ceases to be small and the modulational instability sets in. The modulational instability evolves into wave collapses which are strongly nonlinear singular events shrinking to a very small spatial size in finite time. The collapse dissipates part of the wave-action supplied to it via the inverse cascade, whereas the remaining wave-action returns back to the system of random waves because the collapse spike has a significant high-k component which becomes incoherent when after the collapse burnout.

The qualitative picture of the wave turbulence cycle outlined above can yield to some important qualitative predictions. From the definition of the energy flux in the k-space, ϵ_k, and by taking the first moment of (2.32), we have

$$\dot{E}_k = -\partial_k \epsilon_k = 2\pi k\, \omega_k \int_0^{J_{Ph}} J\, \partial_J F_k \, \mathrm{d}J, \tag{2.36}$$

where we have taken into account the relation $E_k = 2\pi k\,\omega_k\,n_k$ and also the cutoff at $J = J_{Ph}$ that is related to the fact that for $J > J_{Ph}$ the nonlinearity is stronger than the linear terms, which means severe damping via wave breaking (i.e. the gravity force is not able to keep the fluid particles attached to the surface). This leads to the following estimate of the relationship between the the J-flux and the k-flux:

$$F_k \sim \frac{\partial_k \epsilon_k}{2\pi k\,\omega_k\,J_{Ph}}, \tag{2.37}$$

Thus, the intermittent tail of the p.d.f. (2.35) becomes

$$\mathscr{P}_k(J) \approx \frac{F_k}{J\beta_k} \sim \frac{\partial_k \epsilon_k}{2\pi k\,\omega_k\,\beta J\,J_{Ph}} \sim \frac{n_k}{J\,J_{Ph}}. \tag{2.38}$$

Here, we have used the fact that in the kinetic equation

$$\dot{n}_k = \alpha_k - \beta_k n_k \tag{2.39}$$

the two terms on the right-hand side are of the same order.

The p.d.f. tail (2.38) gives the following contribution to the moments of the Fourier amplitudes:

$$M_k^{(p),tail} = \int_0^{JPh} J^p\,\mathscr{P}_k(J)\,\mathrm{d}J \sim \frac{n_k}{p}\,J_{Ph}^{(p-1)}. \tag{2.40}$$

For example, for the ZF states $n_k = n_{ZF}$, we have

$$M_k^{(p),tail} \sim \frac{1}{p}\,\epsilon^{1/3} g^{(p-1)/2}\,k^{1/2-9p/2}. \tag{2.41}$$

On the other hand, the p.d.f. core has a Rayleigh shape,

$$\mathscr{P}_k(J) \approx \frac{1}{n_k}\,\mathrm{e}^{-J/n_k},$$

which corresponds to Gaussian statistics of the wave field. The core part gives the following contribution to the moments:

$$M_k^{(p),core} = p!\,n_k^p. \tag{2.42}$$

For the ratio of the tail and core contributions we have

$$M_k^{(p),tail}/M_k^{(p),core} \sim \frac{1}{pp!}\,(J_{Ph}/n_k)^{(p-1)}. \tag{2.43}$$

In particular, for the ZF state

$$M_k^{(p),tail}/M_k^{(p),core} \sim \frac{1}{pp!}\left(\frac{k}{k_*}\right)^{(1-p)/2}, \tag{2.44}$$

where $k_* = g\epsilon^{-2/3}$.

Thus we can see that for a fixed $p > 1$ and at a fixed k, the p.d.f. tail will dominate in the moments as $\epsilon \to 0$. On the other hand, at fixed ϵ and k, the core will dominate when $p \to \infty$.

3. Experimental set-up

The experiments were conducted in a rectangular tank with dimensions $12 \times 6 \times 1.5$ m filled with water up to the depth of 0.9 m (see figure 3). The gravity waves were excited by a piston-type wavemaker. The wavemaker consists of eight

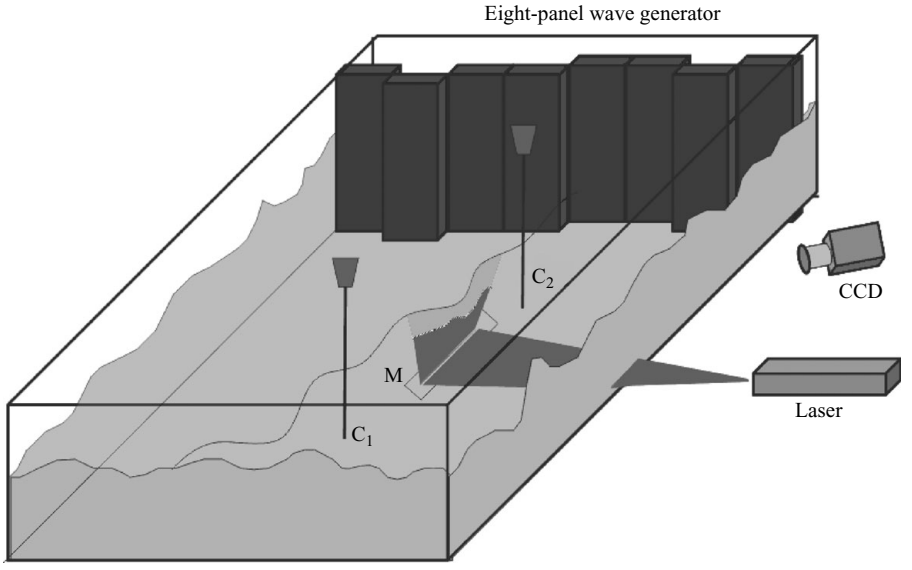

FIGURE 3. The experimental set-up: M, the first surface mirror; C_1 and C_2, the capacitance wire probes; CCD, the digital camera.

vertical paddles of width 0.75 m covering the full span of one short side of the tank. An amplitude, a frequency and a phase can be set for each panel independently, enabling the control of directional distribution of the generated waves. A motion controller is used to programme the parameters of the generated wave field by specifying its amplitude and a number of wave vectors (given by a set of frequencies and directions). In the experiments described here the wavemaker generated a superposition of two waves of equal amplitude with frequencies $f_1 = 0.993$ Hz and $f_2 = 1.14$ Hz (the wavelengths are 1.59 m and 1.2 m correspondingly). The wave vector $\boldsymbol{k}_1$ was perpendicular to the plane of the wavemaker, and $\boldsymbol{k}_2$ was at the angle of 7° to $\boldsymbol{k}_1$. It is assumed that energy dissipation is low, and the waves undergo multiple reflections from the flume walls, interact with each other and form a chaotic wave field homogeneous in the central area of the flume. A choice of the $\boldsymbol{k}$-vectors was motivated by a desire to have a narrow band forcing, which allows a wide inertial range but at the same time leads to a quick phase mixing and isotropization owing to the wall reflections, and does not produce peaks because of the resonances with the flume eigenmodes or harmonics. The main control parameter was an oscillation amplitude of the wavemaker, by varying which we studied the dependence of the spectrum and the p.d.f.s on the average wave intensity.

Two capacitance wire probes were used to measure the wave elevation as a function of time $\eta(t)$ at two fixed points in the central part of the flume (as is shown in figure 3). The distance between the probes was 2 m. Signals from the probes were amplified and digitized by a 16-bit analogue-to-digital converter (NI6035) controlled by the LabView and stored in a PC. Typical signal acquisition parameters were as follows: the bandwidth was 32 Hz, and the recording time was 2000 s. The wire probes were calibrated before the measurements in the same tank with a stationary water surface.

In addition to the measurements of the time dependance, in the present work we have introduced a new technique, similar to that described by Mukto, Atmane &

Loewen (2007), which allows us to measure the dependence of the surface elevation on the space coordinate along a line. For this we used a vertical cross-section image of the air–water interface. The upper layer of water was coloured by the fluorescent dye Rhodamine 6G. The water–air interface area was illuminated from below by a narrow light sheet from a pulsed Yag laser (power 120 mW, wavelength 532 nm; see figure 3). The images were captured by a 1.3 Mpixel digital camera (A622f, Basler) synchronously with laser pulses at the sampling frequency 8 Hz. The image size is 900×1200 mm with the resolution 0.93 mm pixel^{-1} and 0.90 mm pixel^{-1} in the vertical and the horizontal direction respectively. Typically, we collected five sets of images, each set consisting of 240 frames. The time interval between the sets was 5 min. As an example we present in figure 4 a sequence of frames demonstrating an evolution of surface waves.

The data from the capacitance probes were acquired continuously and in parallel with the images during this time. The measurements were done at fixed excitation parameters. The measurement procedure included setting the amplitude of the wavemaker oscillations, waiting for a transient time interval, 20–30 min, and recording the signals during 35 min.

The data were processed using the Matlab. The wire probe data were filtered by a band-pass filter within the frequency band of 0.01–20 Hz. The image sets were processed using standard binarization and the boundary detection procedures from the Image Processing Toolbox. Detected air–water boundaries were stored as a set of arrays, $\eta(x)$, for a following statistical analysis. The images in which the boundary was not a single-valued function of x or had significant jumps ($|\delta\eta(x)|/\delta x| > 4$) were deleted. The proportion of such images was less than 3 %. To calculate spectra from wire probes we used the Welch algorithm with the Hamming window and the averaging performed over 1000 spectral estimates for each signal record. The k-spectra were calculated for each array of boundaries (one array from each image) and then averaged over a set from up to 1200 images for each stationary wave field.

As a characteristic of the averaged wave strength we used a nonlinearity parameter which is defined as the mean slope of the wave at the energy-containing scale, $\gamma = k_m A$, where A is the root mean square (r.m.s.) of η and k_m is the wavenumber corresponding to the maximum of the energy spectrum $|\eta_\omega|^2$. In all our experiments k_m was approximately the same and was located in the forcing range, $k_m \approx 5.2$ m^{-1}, that corresponds to the wavelength $\lambda \approx 1.2$ m. In this experiment the range of the nonlinearity parameter was $0.1 < \gamma < 0.25$.

4. Results

4.1. *Spectra*

Typical energy spectra in the ω-domain and k-domain are shown in figure 5. For the ω-spectra we usually have about one decade of the fitting range, which, according to the dispersion relation, should correspond to the two decades for the k-spectra. In reality the k-spectra have shorter scaling range which is limited, on the low-k side, by the width of laser sheet, 1.2 m, and on the high-k end by insufficient vertical resolution of the images and limited statistics. In addition, the scaling ranges get narrower for the flume runs with weaker forcing.

The slopes of the energy spectra in the ω-domain and k-domain as functions of the wave field intensity are shown in figure 6. We see that for both ω-spectrum and k-spectrum the slopes are steeper for the weaker wave fields with respect to

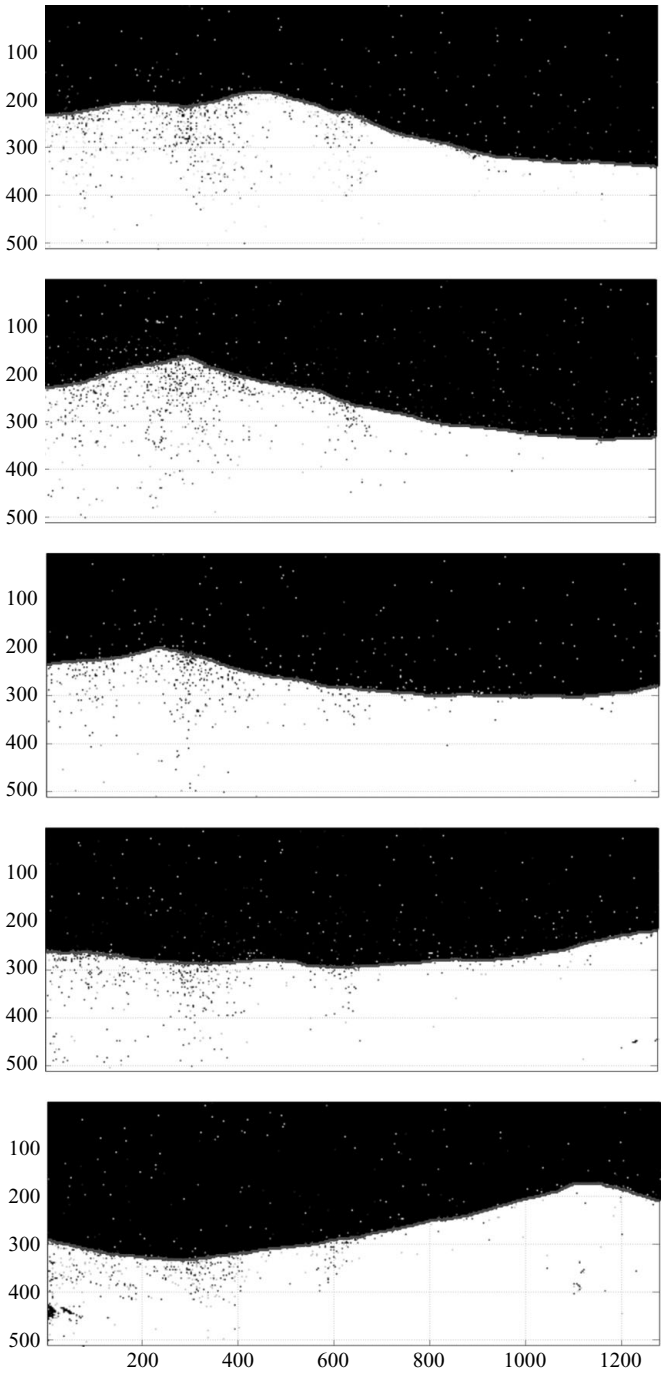

FIGURE 4. A consecutive set of frames showing time evolution of the air–water interface recorded with the sampling frequency 8 Hz, $\gamma = 0.2$.

the stronger ones. One can see that at low wave intensities the data scatter and uncertainty is much greater than for stronger wave turbulence, in agreement with the previous measurements of the ω-spectra in the work of Denissenko *et al.* (2007).

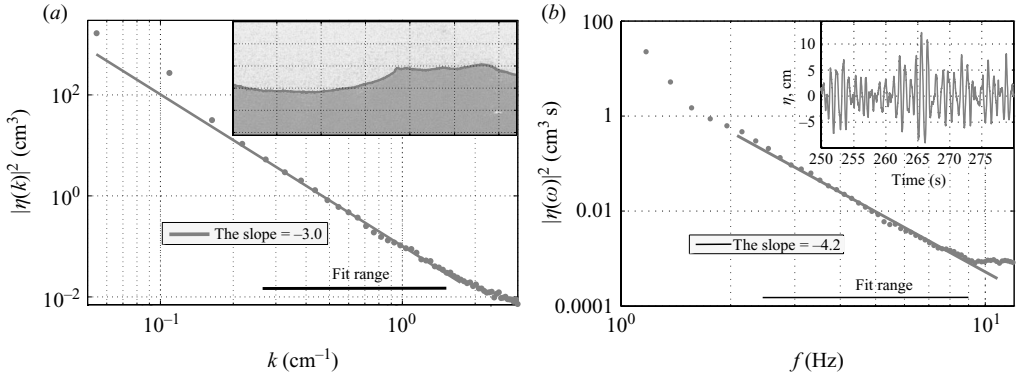

FIGURE 5. (*a*) The spectrum in k-domain. The inset shows an image of the air–water interface. (*b*) The spectrum in ω-domain. The inset shows a correspondent function $\eta(t)$. Both spectra were measured at the wave nonlinearity $\gamma = 0.2$.

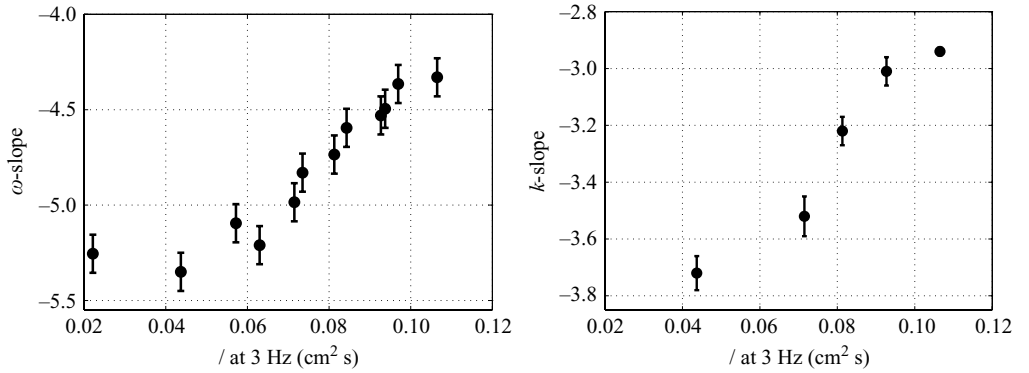

FIGURE 6. Slopes of the k-spectrum and ω-spectrum as functions of the wave intensity I defined as the value of the ω-spectrum of η measured at the frequency 3 Hz, i.e. $I = \langle |\eta_\omega|^2 \rangle_{\omega = 3\,\mathrm{Hz}}$.

In figure 7 we show the graph of the k-slope versus the ω-slope for the energy spectra measured in the same experiments with the laser sheet and the capacitance wire techniques respectively. The data points denoted by the filled and opened circles correspond to two different orientations of the laser light sheet. The solid circular points were obtained with the laser sheet perpendicular to the wavemaker plane as shown in figure 3, and the points denoted by the open circle were obtained with the laser sheet inclined at 20° to the wavemaker. Relatively small differences between these two data sets demonstrate a degree of wave field isotropy. The solid line with the 0.5 slope marks the points for which the k-slopes and the ω-slopes are related via the linear dispersion relation, i.e. $\nu = 2\mu - 1$. As we can see, the experimental data deviate significantly from this line, which indicates that at least in the fitting ranges of scales, the nonlinearity is not weak.

We also plot the points corresponding to the theoretical predictions: Phillips, ZF and Kuznetsov spectra. We see that both Phillips and Kuznetsov points are rather far from the experimental data, whereas the ZF point is more in agreement with the experiment. Namely, this plot suggests that if one would perform experiments at even higher amplitudes, then it is quite likely that the experimental data would have crossed

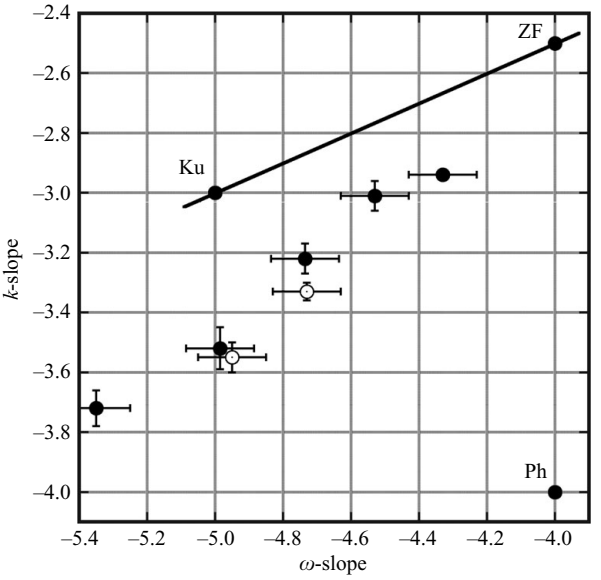

FIGURE 7. The k-slope versus the ω-slope. The solid line marks the points for which the k-slopes and the ω-slopes are related via the linear dispersion relation. Ph, ZF and Ku mark the points corresponding to Phillips, ZF and Kuznetsov predictions respectively. The experimental points shown as the filled circles were obtained from measurements with the light sheet plane oriented perpendicular to the wavemaker plane. The points shown as the open circles were obtained from measurements with light sheet rotated by 70°.

the ZF point. This result is rather surprising because one would naturally expect the ZF theory to work better for weaker rather than for stronger waves. However, as we mentioned before, the finite-flume-size effects are more important for weaker waves, which is the most likely explanation as to why there is a significant deviation from the ZF spectrum at smaller wave amplitudes. Note that the simultaneous measurement of the k-spectra and ω-spectra allows one to resolve the uncertainty of the previous results that have reported on the the ω-spectra only. Namely, we are now able to differentiate between the ZF and Kuznetsov states which have undistinguishable ω-slopes but different k-slopes. The result is that the ZF spectrum is more in agreement with the experimental data than the Kuznetsov spectrum. However, as we will see, coherent singular structures of the type discussed by the Kuznetsov theory do seem to leave their imprints on the scalings of the high-order SFs.

4.2. *The p.d.f.s of the height increments*

To present results on the p.d.f.s and SFs we select the experimental run with the spectra $E_k \sim k^{-3.02}$ and $E_\omega \sim \omega^{-4.2}$. Because for each of these spectra both k-slopes and ω-slopes are steeper than -3 but shallower than -5, we choose to work with the second-order increments, $j = 2$. Experimental p.d.f.s of the height increments in space and time are shown in figures 8(a) and 8(b) respectively. For the space increments, one can clearly see deviations from Gaussianity at the (fat) p.d.f. tails which are related to intermittency and indicate presence of the coherent structures. For the time increments, the deviations from Gaussianity is much less pronounced, which could be due to the slow propagation speed of the coherent structures leading to their more infrequent occurrence in the t-domain in comparison with the x-domain. Both t- and

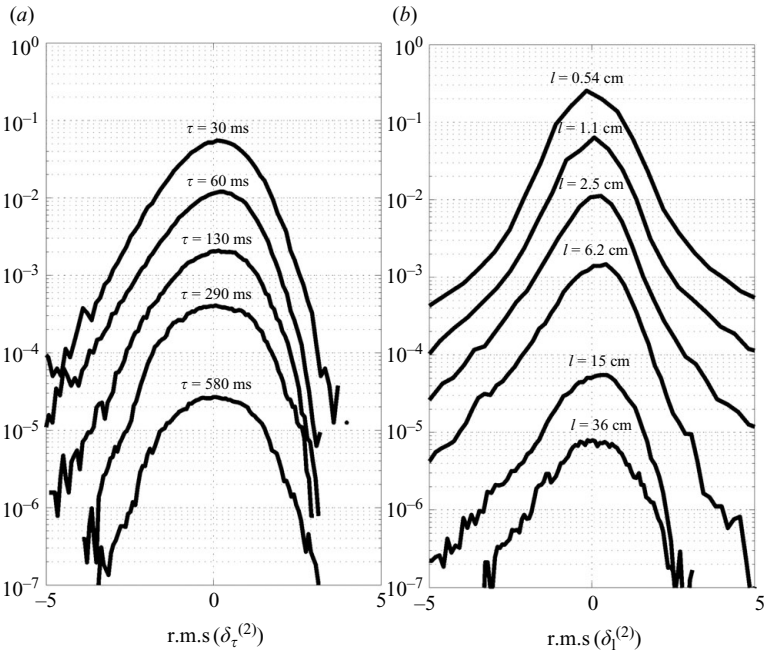

FIGURE 8. The p.d.f.s of second-order differences (*a*) in the *t*-domain and (*b*) in the *x*-domain.

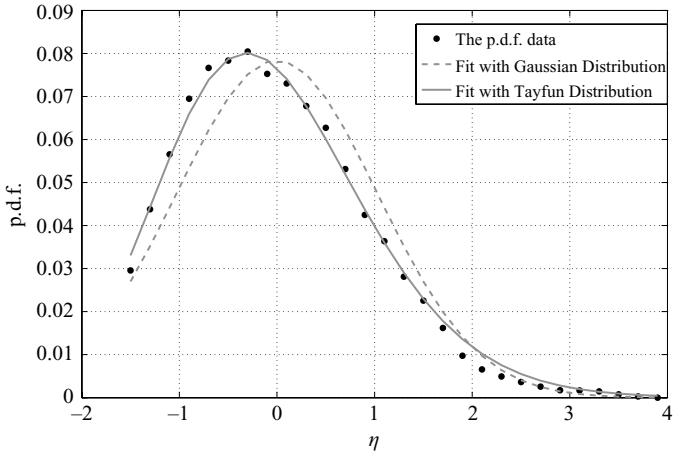

FIGURE 9. The p.d.f.s of the wave elevation η (scaled with standard deviation) compared with the Tayfun distribution (solid line) and the Gaussian distribution (dashed line).

x-domain p.d.f.s are asymmetric (with the negative increments dominant), which results from breaks occurring at wave crests rather than troughs.

Asymmetry with respect to the crests and the troughs is also seen in the one-point p.d.f. of the surface elevation shown for the same run in figure 9. One can see a fatter tail on the right, which corresponds to the typical wave structure in which the crests deviate from the mean elevation more than the troughs. The values of the skewness and kurtosis obtained from this p.d.f. are 0.4 and 3.3 respectively. Also in figure 9 we show a fit of the p.d.f. with Tayfun distribution (2.29), which appears to work quite well in this case.

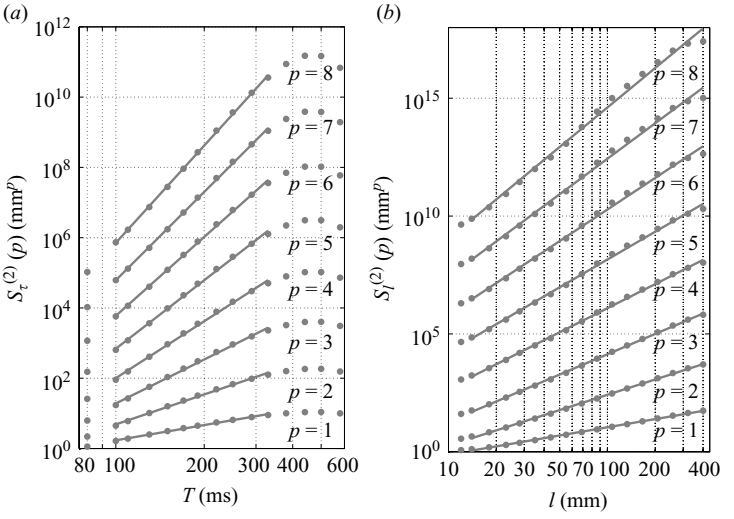

FIGURE 10. The elevation SFs (moments) from the second to eighth order ($p = 2, \ldots, 8$) (a) in the t-domain, $S_\tau^{(2)}(p)$, and (b) in the x-domain, $S_l^{(2)}(p)$, as the functions of τ and l respectively.

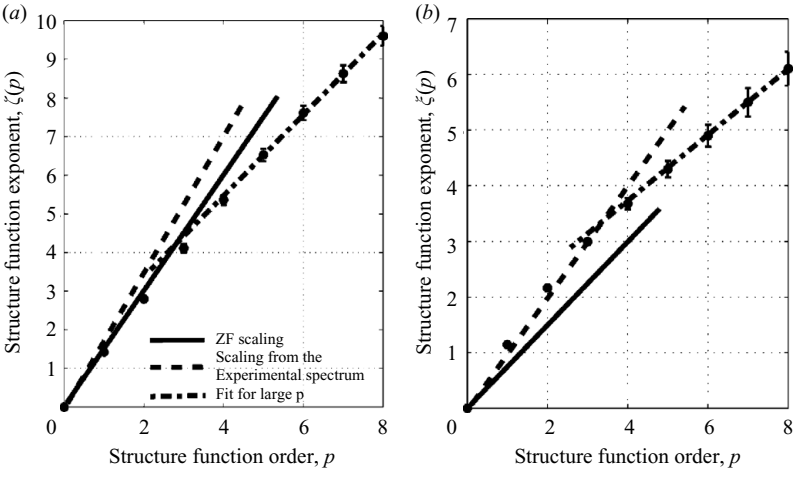

FIGURE 11. SF scaling exponents: (a) $\zeta(p)$ in the t-domain and (b) $\xi(p)$ in the k-domain.

4.3. *Structure functions*

In our data on the SFs, both $S_\tau^{(2)}(p)$ as a function of τ and $S_l^{(2)}(p)$ as a function of l exhibit clear power-law scalings in the range of scales corresponding to the gravity waves for all p at least up to the eighth order (see figure 10). The SF exponents for the time and space domains are shown in figures 11(a) and 11(b) respectively. Straight lines in these graphs represent the ZF scaling (solid line), scaling of waves with the spectrum as measured in the experiment (dashed line) and the fit of the high-p behaviour with a scaling corresponding to singular coherent structures (dash-dotted line). For the time domain, the scaling at low p is close to the ZF scaling; this is surprisingly more consistent than with the scaling calculated from the actual measured spectrum. For an infinite scaling range the $p = 2$ point must, of course, lie exactly on the value corresponding to the spectrum ($\nu - 1$) irrespective of the presence

or absence of the phase correlations. Thus we attribute the observed discrepancy to the finiteness of the scaling range. Furthermore, the fit of the high p dependence indicates the presence of singular coherent structures with $D = 1, a = 1.05$, which is very close to Kuznetsov's $D = 1, a = 1$.

For the space domain, at low p there is an agreement with the scaling of the random-phased waves having the actual measured spectrum and less agreement with the random-phased waves having the ZF spectrum. This is not surprising, since the scaling range in k is greater than in ω, and therefore there is a better agreement between the spectrum and the SF exponent for $p = 2$. More importantly we see again the dominance of the random-phased waves in the low-order SFs and the dominance of coherent breaks in the high-order SFs. The fit at high values of p gives the dimension and the singularity parameter of the breaks $D = 1.3$ and $a = 1/2$ respectively. We see that the breaks appear to be more singular and 'spiky' than the Kuznetsov-type breaks ($a = 1$). Visually, we observed numerous occurrences of these kinds of spiky wave breaks, which are not propagating (or propagating very slowly) and producing vertical splashes. These kinds of structures should be probable in isotropic wave fields owing to the collision of counter-propagating waves, which in our flume appear because of multiple wave reflections from the walls. The slow propagation speed of such breaks means that they seldom cross through the capacitance probe even if they are present in a large number in the x-domain (i.e. more than the Kuznetsov-type breaks). This could explain why the Kuznetsov breaks show up in the SF scalings in the t-domain, whereas more singular spiky structures are seen in the x-domain.

4.4. *Statistics of the Fourier modes*

Let us now present results on the statistics of the Fourier modes. Immediately, we should be cautions about applying the theory of the Fourier mode statistics and intermittency cycle described above in the theoretical part of the paper. Firstly, the theoretical picture was developed for weak waves, where random waves dominate over the coherent structures in most of the inertial range, whereas the experimental runs selected in the present work corresponded to larger excitations, where the r.m.s. amplitude and wave-breaking amplitude are not different by orders of magnitude. Secondly, like the classical WTT, the theory corresponds to an infinite system, whereas the finite-size effects are likely to be important in our flume. Recall that the finite-size effects are strongest at low amplitudes, and it is impossible to implement weak wave turbulence and eliminate the finite-size effects simultaneously in our flume. Thirdly, our statistical data are not sufficient for the single Fourier modes, and as a result, the p.d.f. tails are rather noisy. One can reduce this noise by combining several adjacent Fourier modes, but while doing this one has to be careful not to reduce or eliminate the tail because of such an averaging (i.e. one can only combine modes which are strongly correlated).

Nonetheless, the results in Fourier space p.d.f.s are quite illuminating and worth presenting. The p.d.f.s of ω-modes, $J_\omega = |\eta_\omega|^2$, as measured by the wire probes were first presented in the work of Denissenko *et al.* (2007), and we reproduce them in figure 12. Here, the averaging was done over modes in the frequency range 5.5–6.5 Hz via band-pass filtering. One can see that the p.d.f. core can be fitted with an exponential function which corresponds to Gaussian statistics. At the tail one can see a significant deviation from the exponential fit corresponding to intermittency. As predicted by the theory, the tail follows a power law (with cutoff) but with a different

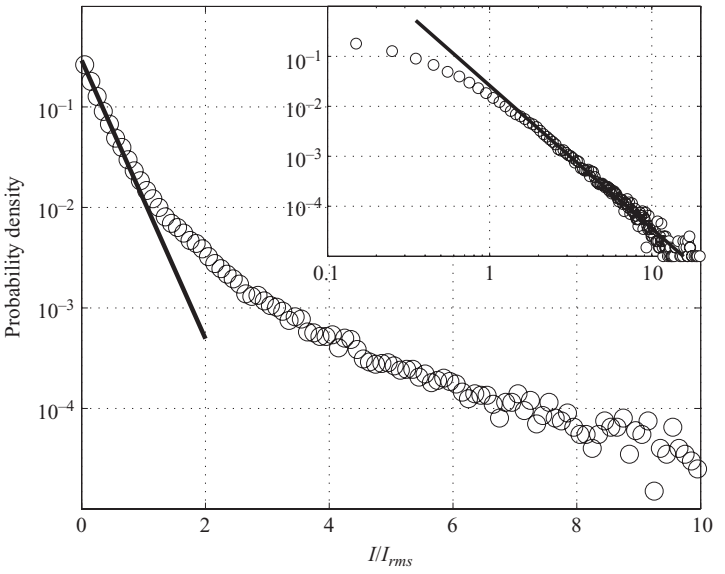

FIGURE 12. Normalized p.d.f. of the spectral intensity $I = |\eta_w|^2$ band-pass filtered with the frequency window ± 1 Hz centred at $f = 6$ Hz, measured at wave nonlinearity $\gamma = k_0 \eta_{rms} \approx 0.16$ (k_0 is the wave vector at the maximum spectral power). The inset shows the same plot in log–log coordinates.

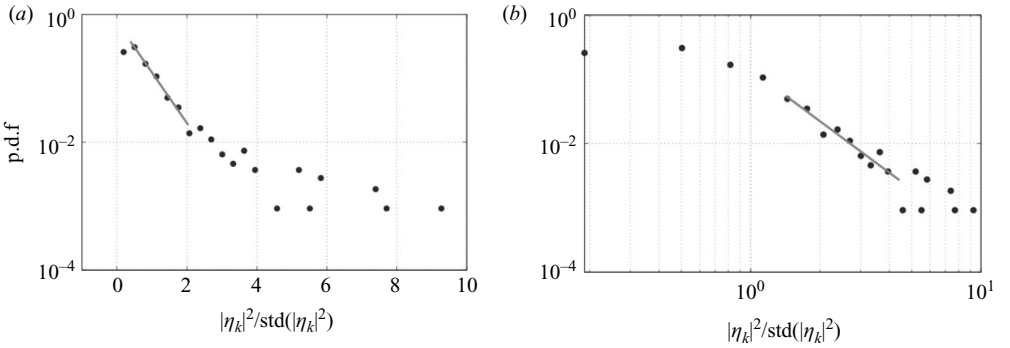

FIGURE 13. The p.d.f. of the k-mode centred at $k = 54.3\,\mathrm{rad\,m^{-1}}$, filtered within the window $\pm 10.8\,\mathrm{rad\,m^{-1}}$ and normalized by its standard deviation. (a) A semilog plot with the exponential fit $y \propto 10^{-1.6x}$. (b) A log–log plot with the power fit $y \propto x^{-2.5}$.

index, -3 rather than -1. This deviation in the power-law index could be due to one of the reasons mentioned at the beginning of this subsection.

The p.d.f.s of k-modes, $J_k = |\eta_k|^2$, are shown in figure 13. Here, the averaging was done over three adjacent modes. Again, we see a Gaussian p.d.f. core and a power-law tail, now with the index -2.5 which is also different from the theoretical index -1. The fact that the p.d.f. tail for the k-modes decays slower than for the ω-modes ($J^{-2.5}$ versus J^{-3}) is consistent with our conclusion (which we have reached based on the statistics of the x- and t-domain increments) that turbulence shows stronger intermittency in space than in time.

It is tempting to interpret the strong deviations from Gaussianity seen in figures 12 and 13 in terms of the 'rogue' or 'freak' waves (for an up-to-date description of

the rogue waves, see Pelinovsky & Kharif 2009). Making such a connection is valid if one believes that the nonlinearity is the main factor in the rogue-wave phenomenon. However, the relation of the Fourier space statistics to the physical space rogue waves is only indirect, and the direct measurements of the surface elevation p.d.f. (like in figure 9) is more appropriate in this case. On the other hand, the Fourier space statistics provides a useful data about the interaction of the random (free) waves and the coherent (bound) waves, as has previously been explained in the current paper. We remind that in this context the power-law tail of the p.d.f. corresponds to the production of the random waves by breaking coherent structures.

5. Summary and discussion

We have presented a theory and performed measurements of gravity wave turbulence statistics in both the x-domain and the t-domain. This has allowed us to differentiate between the states which have the same frequency spectra but different k-spectra, particularly between the ZF and Kuznetsov states. Our data indicate that the spectral exponents, both in ω and k, depend on the amplitude of the forcing. There is a certain evidence favouring ZF theory at larger wave amplitudes, but it is not possible to observe the ZF state in its purity because the two fundamental limits of the WTT, weak nonlinearity and the infinite box, are impossible to implement simultaneously even in such a large flume as ours. None of the existing theories, relying either on the presence of random-phased weakly nonlinear waves or on dominance of coherent wave crests of a particular type, can fully explain our experimental results. Instead, there is an indication that the gravity wave field consists of coexisting and interacting random and coherent wave components, as was earlier speculated based on the open-sea radar measurements of Kudryavtsev *et al.* (2003). The random waves are captured by the p.d.f. cores and the low-order SFs, whereas the coherent wave crests leave their imprints on the p.d.f. tails and on the high-order SFs. The singular wave crests themselves consist of structures of different shapes, namely numerous non-propagating spikes/splashes (which show in the x-domain SFs) and propagating Kuznetsov-type breaks (seen in the t-domain SFs). We suggested a plausible scenario for the dynamics and mutual interactions of these coexisting random-phased and coherent wave components based on a turbulence cycle. Namely, the coherent structures appear in the process of the energy cascade within the random wave component (when the nonlinearity becomes strong at some scale along the cascade). The coherent waves partially dissipate their energy because of wave breaking, and they partially return the energy to a wide range of longer incoherent waves. Based on this, we made qualitative theoretical predictions for the scalings of the moments of the Fourier modes. However, our present statistical data are insufficient for building these moments, and longer experimental runs are needed in future to accumulate this statistics.

As we mentioned before, the finite size of our flume is likely to favour the splash-type breaks over the progressively propagating breaks because reflections from the walls produce counter-propagating waves which collide. The simplest way to understand these splashes is to consider a standing wave with gradually increasing amplitude – at some limiting amplitude the wave nodes will break in a symmetric wave and create an upward jet. The situation is quite different in open seas, where the progressive-wave breaks are dominant. However, we believe that our technique based on SF scalings can be useful in future for analysing the open-sea data in terms of characterizing the properties of the wave-breaking events, as well as their interactions with the random

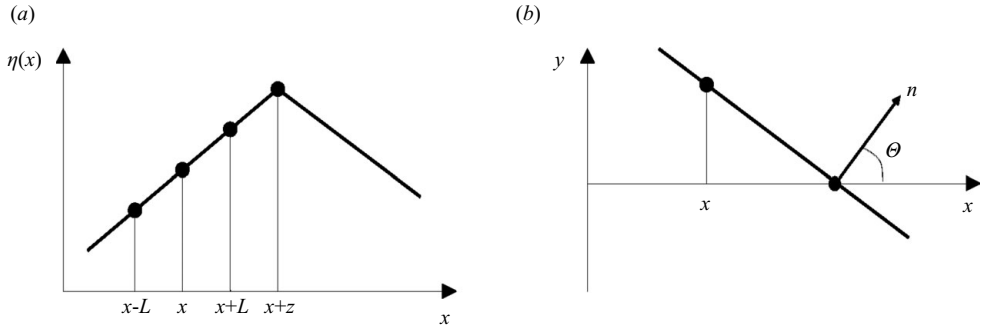

FIGURE 14. Schematic of the ridge (coherent structure) cross-section used in p.d.f. calculations: (*a*) the Kuznetsov-type ridge in the plane $(x, \eta(x))$, where x is directed along the illuminated line on the air–water interface and is parallel to the vector $\boldsymbol{l}$; (*b*) the same ridge in the (x, y)-plane.

wave component. It is also clear that these interactions are the key to understanding the wave turbulence life cycle, and their description should become a priority for the future WTT.

Appendix. The p.d.f.s and the structure functions of singular wave ridges

Let us first ask what shape of the p.d.f. would be produced by structures of the Kuznetsov type with unit slopes on the both sides and $D = 1$. Let us assume that the position and orientation of such ridges are random in the two-dimensional plane. In this case for $j \geqslant 2$, a space height increment will have non-zero values only if it has its argument points on both sides of the coherent structure. Let us restrict ourselves to the $j = 2$ case; then

$$\left.\begin{aligned} \delta_l^{(2)} &= 2\cos\theta\,(l - z), \quad \text{for } |z| < l, \\ \delta_l^{(2)} &= 0, \qquad\qquad\quad \text{for } |z| > l, \end{aligned}\right\} \tag{A 1}$$

where $l = |\boldsymbol{l}|$; the vector $\boldsymbol{l}$ is parallel to the axis x; θ is the angle between the vector normal to the coherent structure's ridge and the vector $\boldsymbol{l}$; and z is the distance from the increment middle point and the intersection between the ridge and the line connecting the increment points (see figure 14).

For the p.d.f. we have

$$P_x^{(2)}(\sigma) = 0, \quad \text{for } |\sigma| > 2l \tag{A 2}$$

(the maximal value of the increment is limited by the strength of the singularity), and

$$\begin{aligned} P_x^{(2)}(\sigma) = \left\langle \delta\left(\sigma - \delta_l^{(2)}\right)\right\rangle &= \frac{1}{\pi}\int_{-\pi/2}^{\pi/2} \mathrm{d}\theta \frac{1}{2l}\int_{-l}^{l} \mathrm{d}z\,\delta(\sigma - 2\cos\theta(l - z)) \\ &= \frac{1}{2\pi l}\int_0^{\arccos\frac{|\sigma|}{2l}} \frac{\mathrm{d}\theta}{\cos\theta} = \frac{1}{2\pi l}\ln\left[\frac{2l}{|\sigma|} + \sqrt{\left[\frac{2l}{|\sigma|}\right]^2 - 1}\right] \end{aligned} \tag{A 3}$$

for $|\sigma| \leqslant 2l$.

In the above, we have considered a simplified configuration of ridges such that on average only one ridge with slope equal to ± 1 crosses a unit area. This result can be easily extended to the structures with a distribution of the slope values and with

an arbitrary density in two-dimensional space. This would move the p.d.f. cutoff to $|\sigma| = 2ls$, where s is the maximal allowed slope of the coherent structures. (Such a p.d.f. cutoff feature was discussed by Choi *et al.* 2005). Asymptotic behaviour for such a general p.d.f. for $|\sigma| \ll 2l$ is

$$P_x^{(2)}(\sigma) \sim \frac{A}{l}\left[\ln\left(\frac{l}{|\sigma|}\right) + B\right], \tag{A 4}$$

where A and B are dimensionless constants which depend on the strength distribution of the singular ridges and their spatial density.

Let us now consider a somewhat more general class of singular coherent structures whose cross-section near the singularity is given by formula (2.24) with a singularity degree such that $0 < a \leqslant 1$ and dimension $0 \leqslant D < 2$ (see figure 1). For the Kuznetsov structures considered above $a = 1$ and $D = 1$.

Contribution to the p.d.f. of the structures with $a < 1$ can be considered as above, and it is easy to see that the corresponding integral of the same type as in the (A 3) is convergent. This means that the structures with $a < 1$ contribute to the p.d.f. tails 'locally'; i.e. structures with amplitudes C_a form a 'bump' on the tail near $\sigma = C_a l^a$. The shape of such a bump is not universal, and it depends on the distribution of the crests over C_a.

On the other hand, an effective way to detect the structures is to consider the SFs and their scalings in l (note that the p.d.f.s are usually measured at fixed values of l, and therefore, the corresponding scalings in l are hard to obtain, e.g. because of insufficient statistical data). We will be interested in the limit $l \to 0$ of the SFs, $S_l^{(j)}(p)$. Suppose that there are N coherent structures per unit area. The probability for having points of the SF on the two different sides of the coherent structure ridge is Nl^{2-D}. The probability to have all the point on the same side of the ridge is $1 - l^{2-D} \approx 1$ (for $l \to 0$). If all the points are on the same side of the ridge then, assuming that away from the ridge the field is j times differentiable, $\delta_l^{(j)} \sim l^j$, whereas if the points are on the different sides of the ridge, $\delta_l^{(j)} \sim l^a$; so

$$S_l^{(j)}(p) \sim l^{pj} + Nl^{2-D+ap}. \tag{A 5}$$

Here, the summation sign is not to be considered literally – it only means that in the limit $l \to 0$, out of the two terms in the sum one should choose the dominant one (i.e. the one with the smallest power).

This work was partially done during the EPSRC-sponsored Warwick Turbulence Symposium programme 2005–2007. The authors are grateful to the Hull Environmental Research Institute for a partial financial support. We thank V. Lebedev for useful discussions and B. Murphy for his help with experiments at the Deep flume.

REFERENCES

Belcher, S. E. & Vassilicos, J. C. 1997 Breaking waves and the equilibrium range of wind-wave spectra. *J. Fluid Mech.* **342**, 377–401.

Choi, Y., Lvov, Y., Nazarenko, S. & Pokorni, B. 2005 Anomalous probability of large amplitudes in wave turbulence. *Phys. Lett.* A **339**, 361–369.

Connaughton, C., Nazarenko, S. & Newell, A. C. 2003 Dimensional analysis and weak turbulence. *Physica* D **184**, 86–97.

Cooker, M. J. & Peregrine, D. H. 1991 Violent water motion at breaking-wave impact. In *Proceedings of the 22nd International Conference on Coastal Engineering (ICCE22, Delft, The Netherlands, July '90)* (ed. M. L. Banner & R. H. J. Grimshaw), vol. 1, pp. 164–176. Springer.

Denissenko, P., Lukaschuk, S. & Nazarenko, S. 2007 Gravity wave turbulence in a laboratory flume. *Phys. Rev. Lett*. **99**, 014501.

Dyachenko, S., Newell, A. C., Pushkarev, A. & Zakharov, V. E. 1992 Optical turbulence: weak turbulence, condensates and collapsing filaments in the nonlinear Schrödinger equation. *Physica* D **57**, 96–160.

Falcon, E., Laroche, C. & Fauve, S. 2007 Observation of gravity–capillary wave turbulence. *Phys. Rev. Lett*. **98**, 094503.

Hasselman, K. 1962 Anomalous probability of large amplitudes in wave turbulence. *J. Fluid Mech.* **12**, 481.

Janssen, P. A. E. M. 2004 *The Interaction of Ocean Waves and Wind*. Cambridge University Press.

Kadomtsev, B. B. 1965 *Plasma Turbulence*. Academic.

Kartashova, E. A. 1991 On properties of weakly nonlinear wave interactions in resonators. *Physica* D **54**, 125–134.

Kartashova, E. A. 1998 Wave resonances in systems with discrete spectra. *Nonlinear Waves and Weak Turbulence – Advances in the Mathematical Sciences* (ed. by V. E. Zakharov), pp. 95–129. *Am. Math. Soc.*

Kitaigorodskii, S. A. 1962 Application of the theory of similarity to the analysis of wind-generated wave motion as a stochastic process. *Bull. Acad. Sci. USSR Ser. Geophys.* **1**, 105–117.

Krasitskii, V. P. 1994 On reduced equations in the hamiltonian theory of weakly nonlinear surface-waves. *J. Fluid Mech.* **272**, 1–20.

Kudryavtsev, V., Hauser, D., Caudal, G. & Chapron, G. 2003 A semiempirical model of the normalized radar cross-section of the sea surface. *J. Geophys. Res* **108** (C3), 8054.

Kuznetsov, E. A. 2004 Turbulence spectra generated by singularities. *JETP Lett*. **80**, 83–89.

Longuet-Higgins, M. S. 1993 Highly accelerated, free-surface flows. *J. Fluid Mech* **248**, 449–475.

Mukto, M. A., Atmane, M. A. & Loewen, M. R. 2007 A particle-image based wave profile measurement technique. *Exp. Fluids* **42**, 131–142.

Nazarenko, S. V. 2006 Sandpile behaviour in discrete water-wave turbulence. *J. Stat. Mech*., 2, 11–18, L02002.

Newell, A. C., Nazarenko, S. & Biven, L. 2001 Wave turbulence and intermittency. *Physica* D **152–53**, 520–550.

Newell, A. C. & Zakharov, V. E. 2008 The role of the generalized Phillips' spectrum in wave turbulence. *Phys. Lett*. A **372**, 4230–4233.

Onorato, M., Cavaleri, L., S. Fouques, O. Gramstad, Janssen, P. A. E. M., Monmaliu, J., Osborne, A. R., Pakozdi, C., Serio, M., Stansberg, C. T., Toeffoli, A. & Trulsen, K. 2009 Statistical properties of mechanically generated surface gravity waves: a laboratory experiment in a three-dimensional wave basin. *J. Fluid Mech.* **627**, 235–257.

Onorato, M., Osborne, A., Serio, M., Cavaleri, L., Brandini, C. & Stansberg, C. T. 2006b Extreme waves, modulational instability and second order theory: wave flume experiments on irregular waves. *Eur. J. Mech.* B **25**, 586–601.

Pelinovsky, E. & Kharif, C. 2009 *Extreme Ocean Waves*. Springer.

Phillips, O. M. 1958 The equilibrium range in the spectrum of wind generated waves. *J. Fluid Mech.* **4**, 426–434.

Socquet-Juglard, H., Dysthe, K., Trulsen, K., Krogstad, H. E. & Liu, J. 2005 Distribution of surface gravity waves during spectral changes. *J. Fluid Mech.* **542**, 195–216.

Tayfun, M. A. 1980 Distribution of surface gravity waves during spectral changes. *J. Geophys. Res.* **85** (C3), 1548–1552.

Tayfun, M. A. & Fedele, F. 2007 Wave-height distributions and nonlinear effects. *Ocean Engng* **34**, 1631–1649.

Toba, Y. 1973 Local balance in the air-sea boundary process. *J. Oceanogr. Soc. Jpn* **29**, 209–220.

Zakharov, V. E. & Filonenko, N. N. 1967 Weak turbulence of capillary waves. *J. Appl. Mech. Tech. Phys.* **4**, 506–515.

Zakharov, V. E., Lvov, V. S. & Falkovich, G. G. 1992 *Kolmogorov Spectra of Turbulence*. Springer.